Journal of Advances in Modeling Earth Systems

RESEARCH ARTICLE
10.1002/2017MS001227

Regional Climate Simulations With the Community Earth System Model

A. Gettelman[1], P. Callaghan[1], V. E. Larson[2], C. M. Zarzycki[1], J. T. Bacmeister[1], P. H. Lauritzen[1], P. A. Bogenschutz[1,3], and R. B. Neale[1]

[1]National Center for Atmospheric Research, Boulder, CO, USA, [2]University of Wisconsin - Milwaukee, Milwaukee, WI, USA, [3]Lawrence Livermore National Laboratory, Livermore, CA, USA

Key Points:
- Comprehensive tests of a variable resolution dynamical core are conducted
- Cloud schemes for CESM2 are not very sensitive to changes in horizontal resolution
- Variable-resolution grids are a viable alternative to traditional nesting for regional climate studies and are available in CESM2

Correspondence to:
A. Gettelman,
andrew@ucar.edu

Citation:
Gettelman, A., Callaghan, P., Larson, V. E., Zarzycki, C. M., Bacmeister, J. T., Lauritzen, P. H., et al. (2018). Regional climate simulations with the Community Earth System Model. *Journal of Advances in Modeling Earth Systems*, *10*, 1245–1265. https://doi.org/10.1002/2017MS001227

Received 1 NOV 2017
Accepted 20 MAR 2018
Accepted article online 25 MAR 2018
Published online 10 JUN 2018

Abstract The spectral element (SE) variable-resolution (VR) mesh dynamical core is tested in developmental versions of the Community Earth System Model version 2 (CESM2). The SE dynamical core is tested in baroclinic wave, aquaplanet and full physics configurations to evaluate variable-resolution simulations against uniform high and uniform low-resolution simulations. Different physical parameterization suites are also evaluated to gauge their sensitivity to resolution. Dry dynamical core variable-resolution cases compare well to high-resolution tests. More recent versions of the atmospheric physics, including cloud schemes for CESM2, are less sensitive to changes in horizontal resolution. Most of the sensitivity is due to sensitivity to time step and interactions between deep convection and large-scale condensation, which is expected from the closure methods. The resulting full physics SE-VR model produces a similar climate to the global low-resolution mesh and similar high-frequency statistics in the high-resolution region. The SE-VR simulations are able to reproduce uniform high-resolution results, making them an effective tool for regional climate simulations at lower computational cost. Some biases are reduced (orographic precipitation in Western United States), but biases do not necessarily go away at high resolution (e.g., summertime surface temperatures). Variable-resolution grids are a viable alternative to traditional nesting for regional climate studies and are available in CESM2.

Plain Language Summary This manuscript describes comprehensive tests of a numerical climate model that has high horizontal resolution in one region. This enables high-resolution simulations of climate, and extreme weather events that occur on small scales to be simulated at lower computational costs. Results indicate that the model represents low-resolution climate well, and also reproduces extreme climate statistics in the region with high resolution. We conclude that the variable resolution model is a good way to simulate and predict regional climate.

1. Introduction

A significant goal of climate simulation is to understand possible impacts of climate change. Many impacts of climate change occur on small scales: such as the scale of a watershed or the synoptic scale of a squall line. It is computationally expensive to resolve these scales, which are on the order of 25 km (0.25°) or less for long integrations of 100 years or more, and only limited simulations have been done (e.g., Small et al., 2014, and references below).

Recently however, high-resolution simulations have become available due to advances in computational power. In uniform high-resolution configurations, the Community Atmosphere Model (CAM) version 5 (Neale et al., 2010) has been run to look at high-frequency climate statistics (Bacmeister et al., 2014; Wehner et al., 2014), including tropical cyclones (Bacmeister et al., 2016), and has also been run coupled to an ocean to look at long-term climate change (Small et al., 2014).

The computational cost of a 0.25° global grid is significant on current high performance computing platforms for long-duration simulations. So "regional climate models" have been developed using typically mesoscale models over limited regions of the planet, to try to reproduce higher-frequency statistics for smaller regions of the globe. These are described in reviews by McGregor (1997), Laprise (2008), and Mearns

et al. (2012) (for regional simulations over the United States), and many others too numerous to list in detail. However, these models must be driven at the boundaries, generally by output from a different lower-resolution global model. This may create significant inconsistencies (Ringler et al., 2011) because the boundary conditions will not match a balanced state of the regional model.

Several studies have begun to investigate another approach to regional climate simulation that uses global models with static variable-resolution (VR) meshes, in which the horizontal size of a grid box changes. These include investigating climate aspects such as tropical cyclones (Zarzycki & Jablonowski, 2014, 2015), orographic forcing (Rhoades et al., 2016; Wu et al., 2017; Zarzycki et al., 2015), and regional precipitation patterns (Harris & Lin, 2013; Huang et al., 2016; Rauscher et al., 2012; Sakaguchi et al., 2015).

This work presents simulations that use the spectral element (SE) dynamical core (Taylor, 2011, and references herein) with variable resolution (VR) in the Community Earth System Model version 2 (CESM2), specifically in the atmospheric component, the Community Atmosphere Model (CAM). The implementation of the SE dynamical core in CAM and the adjustments for CAM6 are described by Lauritzen et al. (2018). Different versions of the CAM physical parameterizations are tested as well. The goal is to evaluate the dynamics and the physical parameterizations of the model with different resolutions and with variable resolution.

This is a test of what is commonly called "scale aware" parameterizations. Scale aware implies the parameterization knows the length scale, which is not true for most physical parameterizations in GCMs. We prefer to state that we are seeking "scale insensitive" parameterizations that at a minimum are robust across uniform resolutions and changes in resolution. Ultimately, we would like the solutions to converge as we refine in the horizontal, vertical and in time. Our study differs from previous work in that it seeks to benchmark VR climate statistics against uniform versions of the same model, and to document the variable-resolution version of the atmosphere for CESM2 and the scale sensitivity of its physical parameterizations.

This study will first explore the dynamics using simplified simulations, then explore different versions of the CAM physics with aquaplanet simulations. Finally, we will analyze "full physics" simulations of the latest version of CAM. We will look at both global and local statistics, and in particular statistics of extreme events. This includes mean climate metrics for surface temperature (*Ts*) and precipitation as well as the variability of precipitation (intensity and diurnal cycle) and extremes of temperature.

The focus is on evaluation of VR grids in CESM2 relative to configurations with uniform high resolution. Can the same climate statistics be achieved at lower cost for metrics that matter by using regional refinement? The central hypothesis of this work is to show that CAM-SE-VR and CESM2 configurations can successfully match uniform high-resolution statistics and be used for consistent regional climate simulations.

Section 2 contains a description of the hierarchy of models used in this study. Results are in section 3 and a summary and conclusions is contained in section 4.

2. Methodology

This section describes the model simulations used in the study. The philosophy follows the evolution of the VR model. First tests are conducted with test cases for midlatitude baroclinic instability. Then aquaplanet simulations are conducted to look at full physics results, first with a refined mesh in the extratropics over a section of longitudes (identical to the baroclinic wave case), and then with a refined mesh in a particular longitude region in the tropics. The aquaplanet tests are done with several versions of the atmospheric model physics as described below. Finally, full physics simulations using a physics suite similar to the final CAM6 physics are conducted with topography and a refined mesh over the Continental United States (CONUS). These different simulations are summarized in Table 1 as they are named in the text.

The model is a developmental version of CAM, the atmospheric component of CESM. The code base contains developmental code for features to be released in CESM2. The atmosphere model uses the spectral element (SE) dynamical core (Taylor, 2011), with the variable-resolution (VR) configuration described in Zarzycki et al. (2014a). The SE dynamical core is tested with several different physical parameterization suites.

Table 1
Table of Simulation Types Used in the Manuscript

Category	Name	Grid	Physics	Hyperviscosity
Dy core test	VRhVR	Variable	Ideal	VR
	VRh30	ne30	Ideal	ne30
	ne30hVR	ne30	Ideal	VR
	ne30	ne30	Ideal	ne30
	ne120	ne120	Ideal	ne120
Aquaplanet	CAM4	Variable	CAM4	VR
	CAM5	Variable	CAM5	VR
	CAM-CLUBB	Variable	CAM-CLUBB	VR
Full physics	VarMesh	Variable	CAM6	VR
	ne30	ne30	CAM6	ne30
	ne120	ne120	CAM6	ne120

Note. VR, variable resolution; ne30, low resolution; ne120, high resolution. Hyperviscosity indicates settings as noted in the text. The standard VR case (VRhVR), ν ranges from 1×10^{13} at 0.25° to 1×10^{15} at 1°, a VR case with a non-scale-selective hyperviscosity appropriate for the ne30 low-resolution case (VRh30, constant $\nu=1\times10^{15}$) and a low-resolution (ne30) case with hyperviscosity option set to the variable-resolution settings (ne30hVR, ν approximately 1×10^{13}).

CAM4 (Neale et al., 2013) is the atmosphere model for CCSM4 (Gent et al., 2011) and CAM5 (Neale et al., 2010) is the atmosphere model for CESM1 (Hurrell et al., 2013). We also use a version of the atmosphere model CAM5 that includes a new unified moist turbulence parameterization, Cloud Layers Unified by Binormals (CLUBB), developed by Golaz et al. (2002) and Larson et al. (2002) and implemented in CAM by Bogenschutz et al. (2013), called CAM5-CLUBB. Finally, we use a version that contains CLUBB plus updated aerosols and cloud microphysics (MG2) described by Gettelman (2015). We call this last version CAM6α.

A series of resolutions were tested, corresponding to a uniform low resolution of ~1° (100 km) on a cubed sphere. This has 30 × 30 elements per cube face and each element has 4 quadrature points in each coordinate direction with duplicate points on the boundaries and is called "ne30." Uniform high resolution has 120 × 120 elements per face (corresponding to ~0.25° or 25 km horizontal resolution), and is called "ne120." The variable mesh simulations have ne120 resolution in the refined region, and adjust smoothly to ne30 outside it. Variable-resolution grids in CESM are generated using the SQuadGen package (Guba et al., 2014), which allows for unstructured, user-specified refinement configurations on a base cubed-sphere grid. Topography files are generated using the remapping and differential smoothing procedures outlined in Lauritzen et al. (2015) and Zarzycki et al. (2015), respectively.

A grid with regional refinement over the Continental United States (CONUS) is shown in Figure 1. The time step of ne30 simulations is 1,800 s, and the time step for ne120 simulations is 900 s. Variable-resolution simulations use a time step of the highest resolution (i.e., 900 s for an ne120 refined region). Vertical resolution is 30 levels up to 3 hPa, with finer resolution of ~0.2 km near the surface, expanding to ~1 km near the tropopause, to 2–3 km near the model top.

Variable-resolution CAM-SE has been shown to scale linearly with the relative number of elements of a mesh (compared to a global high-resolution grid) so long as the finest resolution is the same (Zarzycki & Jablonowski, 2014). Therefore, the variable-resolution (ne30 to ne120) costs approximately 10% of the ne120 simulations, a number supported by informal wall-clock estimates of the simulations.

2.1. Dynamical Core Test Case

Dry dynamical core test cases were designed to analyze the dynamics of the spectral element dynamical core using the baroclinic wave test case of Jablonowski and Williamson (2006). The dry dynamical core baroclinic wave test on an aquaplanet was run with (A) uniform high resolution (0.25°, ne120 in the SE nomenclature), (B) uniform low resolution (1°, ne30), and (C) a VR case with a high-resolution region was placed from 25°N to 65°N over 60° of longitude. Simulations were run for 30 days.

Dry dynamical core test case simulations were also used to test the internal damping in the SE core to verify that the damping itself is not affecting results with changes in resolution. The SE dynamical core uses a resolution dependent setting for the fourth-order horizontal hyperviscosity operator (ν) to damp waves that

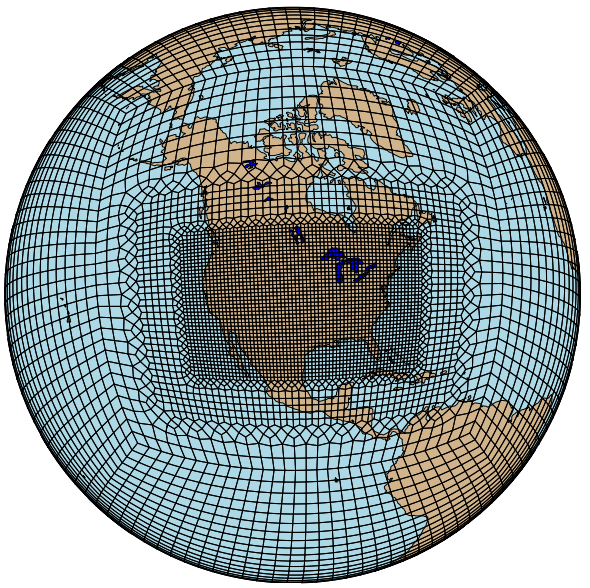

Figure 1. Continental United States (CONUS) variable-resolution mesh for the spectral element (SE) dynamical core.

are not resolvable (Zarzycki et al., 2014a). Different values of hyperviscosity were tested. (1) The standard VR case (VRhVR), ν ranges from 1×10^{13} at 0.25° to 1×10^{15} at 1°, (2) a VR case with a non-scale-selective hypervisocity appropriate for the ne30 low-resolution case (VRh30, constant $\nu=1\times10^{15}$), and (3) a low-resolution (ne30) case with hyperviscosity option set to the variable-resolution settings (ne30hVR, ν approximately 1×10^{13}).

2.2. Aquaplanet

Next, simulations were performed using the full physical parameterization suite for the atmosphere, but with a uniform "aquaplanet" land surface. These simulations place a variable mesh (a) in the midlatitudes from 25°N to 65°N as with the baroclinic wave case and (b) with a tropical mesh from 30°S to 30°N and over 60° of longitude. These simulations were designed to test physical parameterization suites and were performed with CAM4, CAM5, and CAM5-CLUBB physical parameterizations. Note that CLUBB actually knows the grid box size and uses this information to truncate the turbulent length scale. Simulations were run for 3 years under uniform equinox conditions. The high-resolution portion of the nest is at 0.25° (ne120) with the low-resolution portion at 1° (ne30). ν ranges from 1×10^{13} in the high-resolution region to 1×10^{15} in the low-resolution domain. The physics time step is 900 s.

2.3. Full Physics Simulations

Finally, full physics simulations were run with the CAM6α configuration, including the physical parameterizations for CAM6, which is a similar configuration as CAM5-CLUBB. Simulations were run with uniform ne120 (high resolution, 0.25°, ~25 km), and uniform ne30 (low resolution, 1°, ~100 km). Simulations were run for 26 years from 1980 to 2005. The VR mesh has high resolution from 22.5°N to 50°N and 230° to 295° longitude (130°W to 65°W), illustrated in Figure 1. We use a time step of 900 s for all simulations (typically a low-resolution CAM6 simulation would use 1,800 s), and a coupling frequency between the microphysics and CLUBB of 300 s (three couplings per time step), following Gettelman and Morrison (2015). The only modification between the simulations is that to keep the energy more in balance we adjust the critical diameter for ice autoconversion (DCS) in the high-resolution (ne120) simulation only (increase DCS from 140 to 275 μm). This increases high cirrus clouds, compensating for slightly reduced deep convective activity. The climate of midlatitudes is very similar across resolutions, and there is little difference due the change in high cloud parameter. The hyperviscosity coefficient is set to $\nu=1\times10^{15}$ in the ne30 simulation, $\nu=1\times10^{13}$ in the ne120 simulation, and correspondingly scaled as a function of grid size using these base coefficients in the VR run as described for the dynamical core test cases above.

2.4. Observational Comparisons

For comparison to observations with the full physics simulations, we use several different data sets. For climatological comparisons, we use the European Center Interim Reanalysis (ERAI) at ~70 km resolution (Dee et al., 2011). For analysis of the diurnal cycle of precipitation, we use precipitation data from the Tropical Rainfall Measuring Mission (TRMM) (Kummerow et al., 1998) based on TRMM 3B42 0.25° 3 hourly gridded data.

The National Oceanic and Atmospheric Administration (NOAA) Climate Prediction Center (CPC) provides analysis of daily precipitation for the Continental United States at 0.25° by combining rain gauge data with an optimal interpolation objective analysis technique (Chen et al., 2008).

Finally, we also use precipitation and surface temperature daily and 3 hourly from the North American Regional Reanalysis (NARR). NARR is a high-resolution (32 km, 3-hourly) reanalysis product dynamically downscaled over N. America (Mesinger et al., 2006).

All data are concurrent in time with model simulations (1980–2005). Full physics and terrain model simulations follow the protocol for Atmospheric Model Intercomparison Project (AMIP) simulations with monthly mean observed ocean temperature and observed aerosol and trace gas emissions from 1979 to 2005 as boundary forcing. The first year is not analyzed. Land temperatures are prognostic. As a result, high-frequency variability in the model simulations will not correspond to any particularly observed weather event.

3. Results

3.1. Baroclinic Wave Test Case

Figure 2 illustrates the level 2 (L2) Error Norms of the 850 hPa temperature field for various configurations using the uniform resolution 0.25° (ne120) case as the reference. L2 error norms are a root-mean-square error approach to evaluate symmetry deviations from the zonal average. L2 error norms are defined as in Jablonowski and Williamson (2006). The nonzero values for VRhVR at $t = 0$ are a result of interpolation because the uniform ne120 grid values are not aligned with the ne120 gridpoints in the refinement region sampled. The initial flat phase to day 7 or so with different viscosity indicates different damping of the initial disturbances.

The key feature is that out to 8 days or so the variable mesh simulation with appropriate damping (setting the hyperviscosity for variable mesh settings, VRhVR) has low L2 error scores inside the region of refinement (low error norm relative to the reference uniform ne120 high resolution) compared to other cases. This shows regional refinement maintains fine-scale structure of features and is similar to other dynamical cores (Jablonowski & Williamson, 2006, Figure 10). When the hyperviscosity is set to the globally uniform low-resolution coefficient (VRh30), results are not as satisfactory, implying that the additional explicit diffusion is damping any improved resolvable scales in the high-resolution nest. Setting the hyperviscosity in an ne30 case to the variable-resolution settings (ne30hVR) produces a very similar result to uniform low resolution, which is expected since the variable-resolution hypervisocosity scaling in Zarzycki et al. (2014a) is designed to match the uniform configuration when unrefined grids are utilized within the variable-resolution framework. This also further confirms appropriate behavior of the scaling mechanism used for variable-resolution runs when compared to standard uniform resolution configurations. Error norms for all configurations eventually all converge to similar values in agreement with Ringler et al. (2011), who found that analytic errors are eventually constrained by the lowest resolution of a variable-resolution mesh, not the refined patch.

Figure 2 illustrates that the variable mesh matches uniform high-resolution temperature error norms in the high-resolution region, consistent with the findings in Zarzycki et al. (2014b). Evaluation of surface pressure perturbations Figure 3 indicates that VR simulations in the low-resolution region in midlatitudes downstream of the breaking wave look like the high-resolution simulation. Specifically the differences between uniform high resolution (ne120) and low resolution (ne30) in Figure 3a outside the high-resolution region, look like differences between variable mesh (VRhVR) and low resolution Figure 3b. Thus, once waves are generated in the high-resolution region, they propagate as expected into and through the low-resolution region. Scales which are not resolvable in the low resolution are damped as they enter the low-resolution region via the resolution-aware hyperviscosity operator but already-resolved scales generated in the high-resolution nest are allowed to affect the mean flow, even in the low-resolution region.

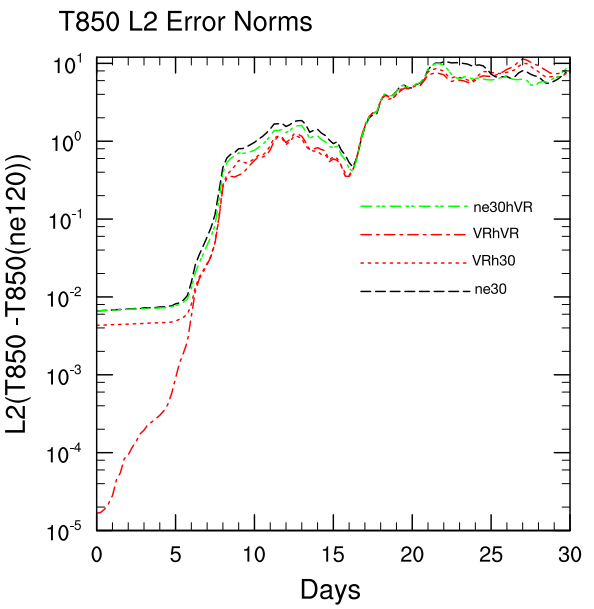

Figure 2. 850 hPa temperature field L2 error norms following Jablonowski and Williamson (2006) inside a region of midlatitude mesh refinement. L2 error norms show the difference from a reference, in this case uniform 0.25° (ne120) resolution, for variable mesh (VRhVR: red dot dash), variable mesh with unscaled ne30 hyperviscosity (VRh30: red dotted), uniform low resolution (ne30: black dash), and uniform low with scaled hyperviscosity (ne30hVR: green dot dash).

However, there is also an upstream effect. Disturbances propagating into the high-resolution from the low-resolution region are damped, such that a picture of day 13, when the baroclinic wave is still in the low-resolution region, has more differences in amplitude between variable resolution and high resolution. This means some care must be taken in positioning the high-resolution region.

3.2. Aquaplanet Simulations

3.2.1. Midlatitude Refinement

Results of the dynamical core test case simulations provide initial confidence in the configuration and in the dynamical core. The next step is to run the aquaplanet model with full physics. This was done for the midlatitude refinement case again. Three different physics packages were used: CAM4, CAM5, and CAM5-CLUBB. The CAM5-CLUBB configuration is an intermediate between CAM5 and CAM6, with the important addition of the CLUBB unified turbulence scheme. Note that all

three configurations use the same basic deep convective scheme (Zhang & McFarlane, 1995, hereafter ZM), with a slightly different closure in CAM5 and CAM5-CLUBB (Neale et al., 2008). But the shallow convective scheme is different in all three: Hack (1994) for CAM4, Park and Bretherton (2009) for CAM5 and CLUBB (Bogenschutz et al., 2010, 2013) for CAM5-CLUBB. Note that CLUBB combines the macrophysics (cloud fraction and large-scale condensation), boundary layer and shallow convection into one scheme that drives stratiform microphysics.

Figure 4 illustrates means in the 25°N–60°N latitude band for zonal mean (blue), inside the refined region (green), and outside (red). Different resolutions (Ne30, Ne120, and Var) are shown at different *x* axis positions. Each of the three physics suites is denoted by a uniquely shaped line marker: CAM4 (square), CAM5 (circle), and CAM5-CLUBB (triangle). Figure 4a illustrates mean cloud fraction. CAM4 (squares) in the variable-resolution configuration (Var) has a large difference in cloud fraction between the region inside and outside the mesh. The error bars represent one standard deviation (σ) of aquaplanet monthly means in a region the size of the variable mesh region and are similar for all simulations ($\sigma \sim$0.02 for cloud fraction). Differences inside and outside the high-resolution region in uniform cases are indicative of variability of the

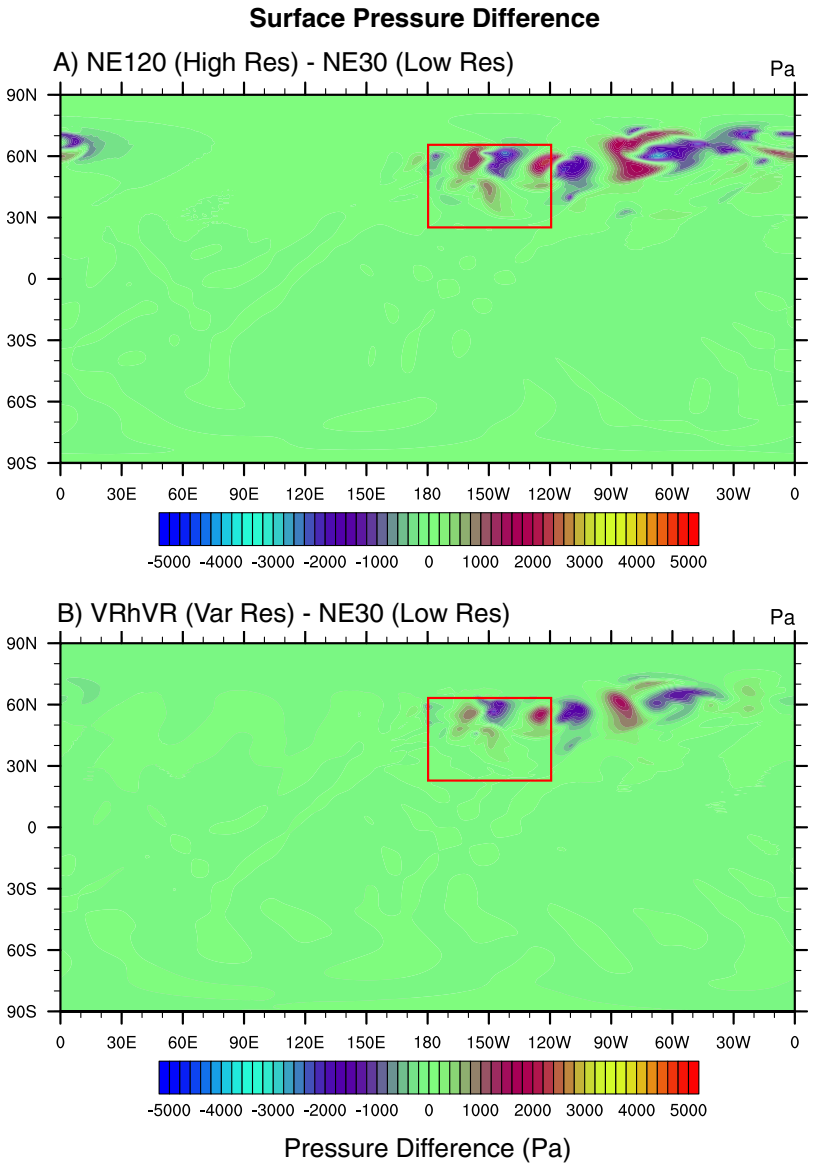

Figure 3. Differences in surface pressure for the idealized case at day 14 for (a) high resolution (ne120) versus low resolution (ne30) and (b) variable resolution (VRhVR) versus low resolution (ne30). The region of refinement is marked in the red box.

physics with scales. CAM4 also has a big difference in cloud fraction (Figure 4a) between Ne120 (high res) or variable mesh at about 0.57 and Ne30 (about 0.67). Thus, CAM4 VR inside the mesh (Var, green) looks like the high resolution (ne120) CAM4 while outside the mesh (red) and zonal mean (blue) look like the low resolution (Ne30) CAM4. This indicates the cloud fraction is dependent on resolution in CAM4. CAM5 (circle) and CAM-CLUBB (triangle) have more similar mean cloud fractions inside and outside the mesh in all cases, and similar results across resolutions.

Figure 4b indicates a similar result for 850 hPa zonal wind speed. The CAM4 solutions vary by almost 3 m s^{-1} between ne30 and ne120. The standard deviation is about 2 m s^{-1} so it is not clear that these differences are significant. Interestingly the VR simulation looks like the low resolution in CAM5. Figure 4c illustrates results for longwave (LW) cloud radiative effects (CRE). The standard deviation is about 2 W m^{-2} in CAM4 (square), cloud forcing differs by 5 W m^{-2} (20%) inside and outside the variable mesh region, and also between resolutions. This is similar to cloud fraction (Figure 4a), since the two fields are related. CAM5 (circle) varies by 2 W m^{-2} and CAM5-CLUBB (triangle) by 0.5 W m^{-2} across resolutions (less than the variability), and the VR simulation tends to look more like the high resolution for CAM5 and CAM5-CLUBB. There is little difference inside and outside the high-resolution region for CAM5 and CAM5-CLUBB. Finally, Figure 4d illustrates similar results for shortwave cloud radiative effects (SWCRE). The standard deviation is about 4 W m^{-2}. There is more variation in SWCRE across resolutions in all the configurations, but for CAM5-CLUBB and CAM4, the VR simulation is closer to the high resolution, and results are similar inside and outside the VR region for CAM5 and CAM5-CLUBB.

In general, CAM5 and CAM5-CLUBB are quite stable in midlatitude cloud systems, and vary little in any single run inside or outside the high-resolution region. CAM4 however has a strong resolution dependence, consistent with previous findings (Rauscher et al., 2012; Williamson, 2008; Zarzycki et al., 2014a).

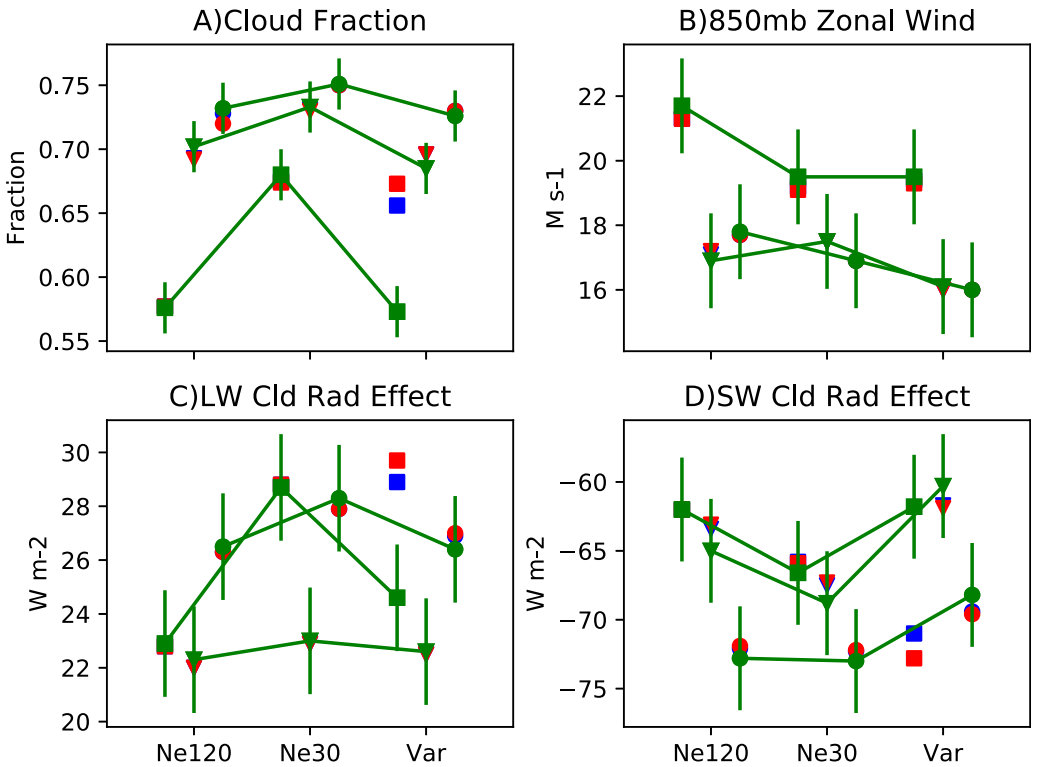

Figure 4. Mean 25°N–60°N statistics from Aquaplanet experiments. Zonal mean (blue), inside the refined region (green), and outside (red). Nine different simulations are shown. Three different resolutions shown as different *x* axis positions: uniform 0.25° (ne120) resolution, uniform low (1°) resolution (ne30), variable mesh (Var) with a slight x shift for each of three physics configurations: CAM4 (square), CAM5 (circle), and CAM-CLUBB (triangle) for clarity of seeing the different symbols. The lines connect the different values across resolutions for the refined region means. Error bars show one standard deviation of monthly means in the refined mesh region.

3.2.2. Tropical Refinement

Experiments have been conducted with a refined mesh region in the tropics, again using an aquaplanet configuration. The mesh is centered on the equator and extends 60° of longitude and from 30°S to 30°N latitude. This is indicated as the red lines in Figure 5.

Figure 5 presents a map of the mean tropical precipitation rate from these variable mesh simulations. CAM4 (Figure 5c) has high precipitation in the refined region over the equatorial intertropical convergence zone, CAM5 (Figure 5b) has less precipitation in the high-resolution region and is more uniform, and CAM5-CLUBB (Figure 5a) has high precipitation both inside and outside the high-resolution region. The total precipitation (PRECT) is more similar inside and outside the high-resolution region along the equator in CAM5-CLUBB (Figure 5a) than in the other configurations (Figures 5b and 5c). The corresponding average values along the equator are illustrated in Table 2.

Figure 6 illustrates that in all three simulations, as expected, the ratio of large-scale (PRECL: Figures 6a–6c) to convective (PRECC: Figures 6d–6f) precipitation is greater inside the high-resolution region than in the outer, low-resolution region. The time step is the same in both regions, so the convective relaxation time in relation to the time step is the same. But the equatorial vertical velocity forcing supersaturation for the large-scale condensation is higher in the high-resolution region, driving more condensation. This has been verified by looking at the vertical pressure velocity (ω) field, where in the region of refinement, there are 30% higher vertical velocities, similar to uniform high-resolution simulations. Since the condensation in the macrophysics is generally not limited with a time scale, it removes water right away. This would increase stratiform precipitation in the refined regions, as seen in all cases in Figure 6 and Table 2. And more condensation done by the stratiform scheme with fixed precipitable water means less available for convection, so convective precipitation is lower inside of the refined region (Table 2).

The compensation between convective (PRECC) and large-scale (PRECL) precipitation occurs in all three schemes, but in CAM5-CLUBB (Figures 6a and 6d) and CAM5 (Figures 6b and 6e) there is less variation in total precipitation inside and outside the high-resolution region than in CAM4 (Figures 6c and 6f). This is illustrated in Table 2. This is an important property since VR aquaplanet configurations where total precipitation varies greatly between high-resolution and low-resolution regions can drive spurious Gill-type circulations associated with asymmetric latent heating as a function of longitude (Rauscher et al., 2012; Zarzycki et al., 2014a).

Finally, we show sets of vertical profiles of the different physics tendency terms averaged 5°S–5°N inside (solid lines) and outside (dashed lines) the high-resolution region. Figure 7 shows temperature (T) and Figure 8 illustrates specific humidity (Q) tendencies. The different terms are for the total physics tendency (black: DTCOND and DCQ for temperature and humidity, respectively), the macrophysics and microphysics

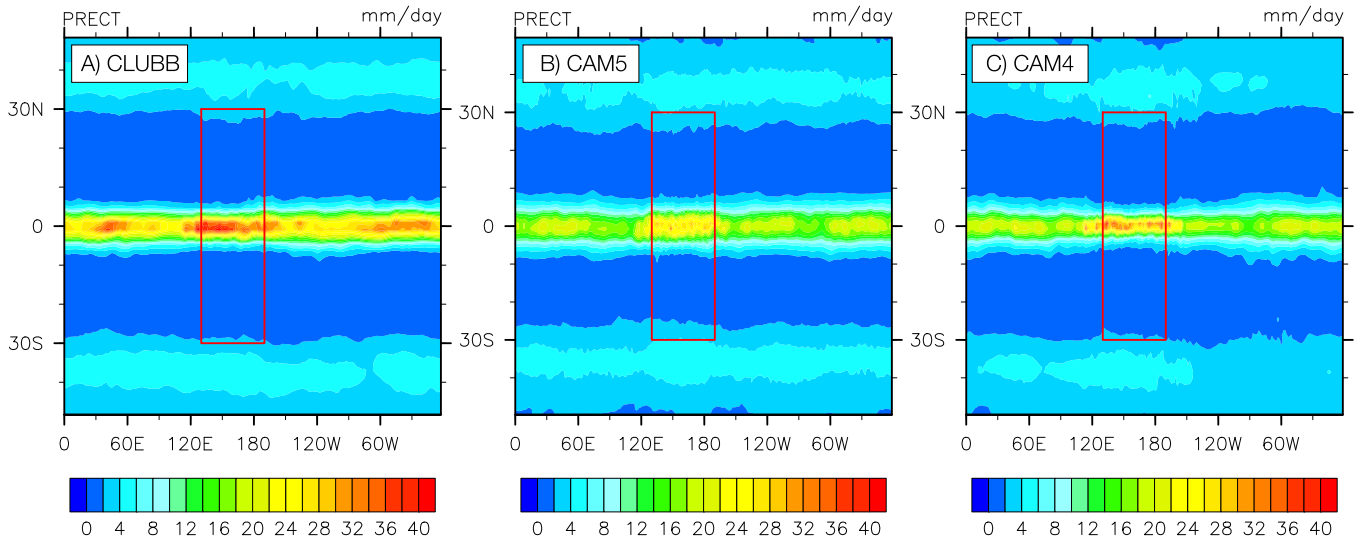

Figure 5. Total mean tropical precipitation rate (mm/d) from variable mesh aquaplanet simulations with different physics packages: (left) CAM-CLUBB, (middle) CAM5, and (right) CAM4. The red box indicates the boundaries of the high-resolution region.

Table 2
Average Precipitation in mm d^{-1} From Aquaplanet Simulations Along the Equator (5°S–5°N) for Different Physics Configurations Inside and Outside the Region of Refinement for Convective (PRECC), Large-Scale (PRECL), and Total (PRECT) Precipitation

Type	Physics	Inside	Outside
Convective	CAM4	8	12
	CAM5	10	15
	CAM5-CLUBB	14	18
Large scale	CAM4	20	6
	CAM5	18	5
	CAM5-CLUBB	22	10
Total	CAM4	28	18
	CAM5	28	20
	CAM5-CLUBB	36	28

(blue: MPDT and MPDQ, this includes all condensation from CLUBB), the shallow convection (red: CMFDT and CMFDQ: note that CLUBB does not have any separate shallow convection and so the red lines are zero and their contributions are included in MPDT and MPDQ) and tendencies for the deep convection (green: ZMDT and ZMDQ). Note that the budgets will not totally balance due to diffusion and other small terms.

The temperature tendencies in Figure 7 indicate similar results to the mean tropical precipitation figures (Figures 5 and 6). There is a difference in deep convective (green) and large-scale (blue) precipitation inside (solid) and outside (dashed) the high-resolution region. This occurs in most of the simulations, with shallow convection differing the most in CAM4 (Figure 7c). Note that the CAM5-CLUBB simulation (Figure 7a) has more constant total tendencies inside and outside the high-resolution region than the other two configurations for strati-

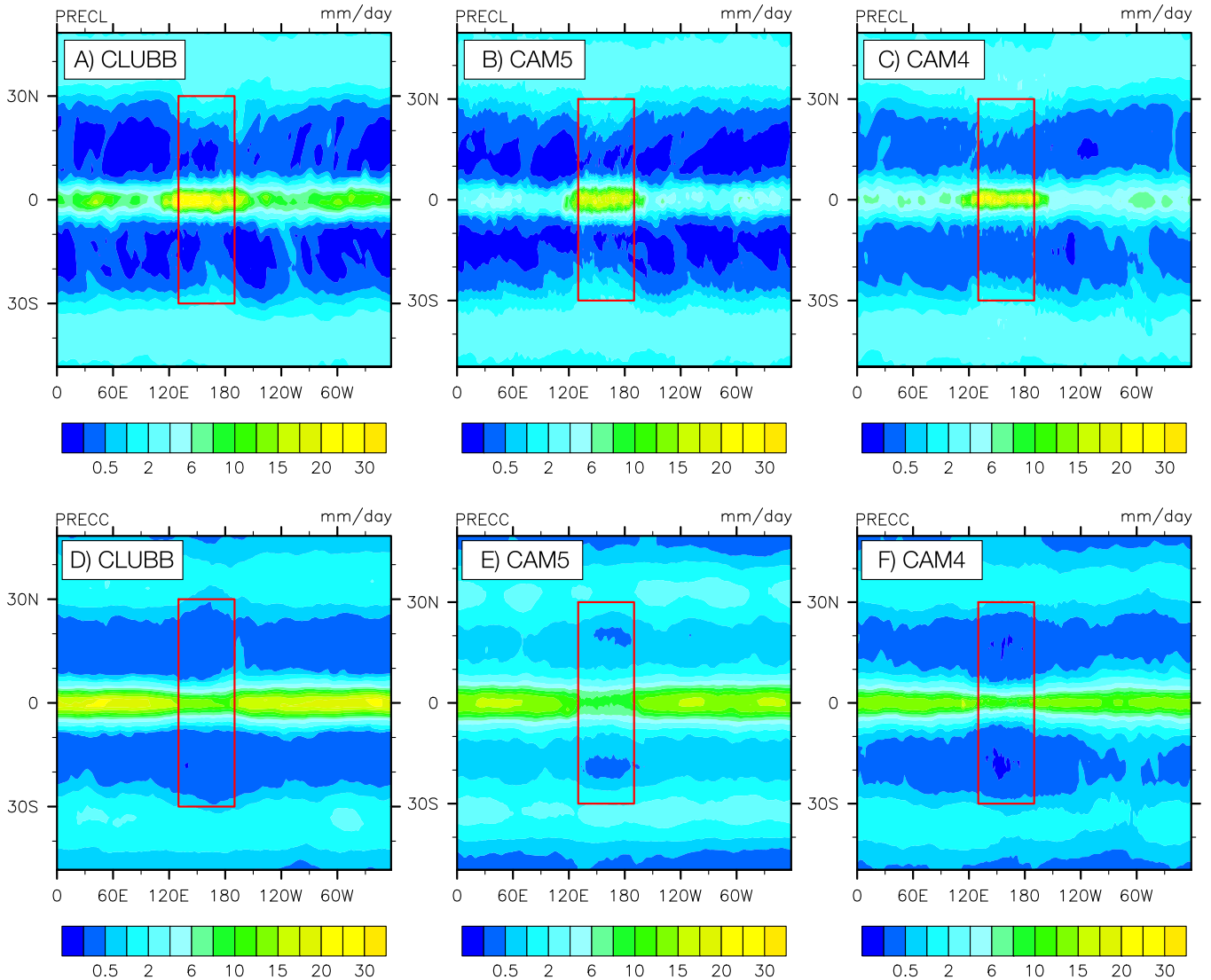

Figure 6. Tropical precipitation rates as in Figure 5 from variable mesh aquaplanet simulations. (top row) Large-scale precipitation and (bottom row) convective precipitation. The red box indicates the boundaries of the high-resolution region.

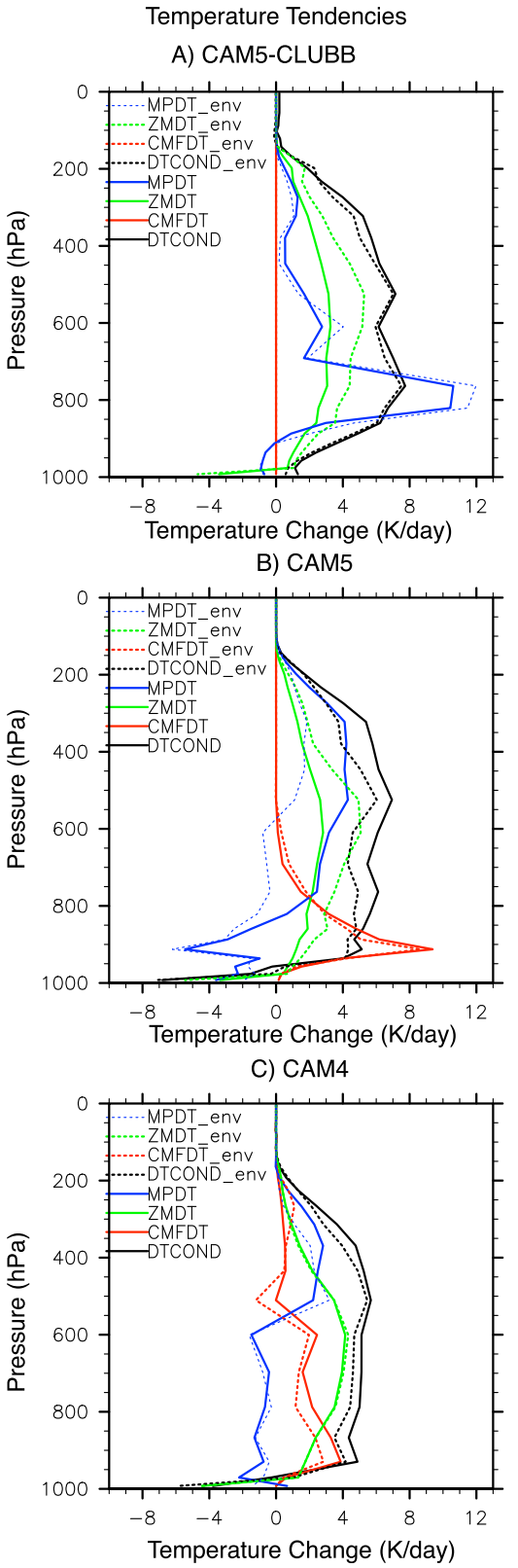

Figure 7. Temperature tendency profiles from (a) CAM-CLUBB, (b) CAM5, and (c) CAM4 averaged over 5°S–5°N inside (solid) and outside (dashed) the region of refinement. The tendency terms are deep convection (ZMDT: green), shallow convection (CMFDT: red), large scale (macro and micro: MPDT blue), and total (DTCOND: black).

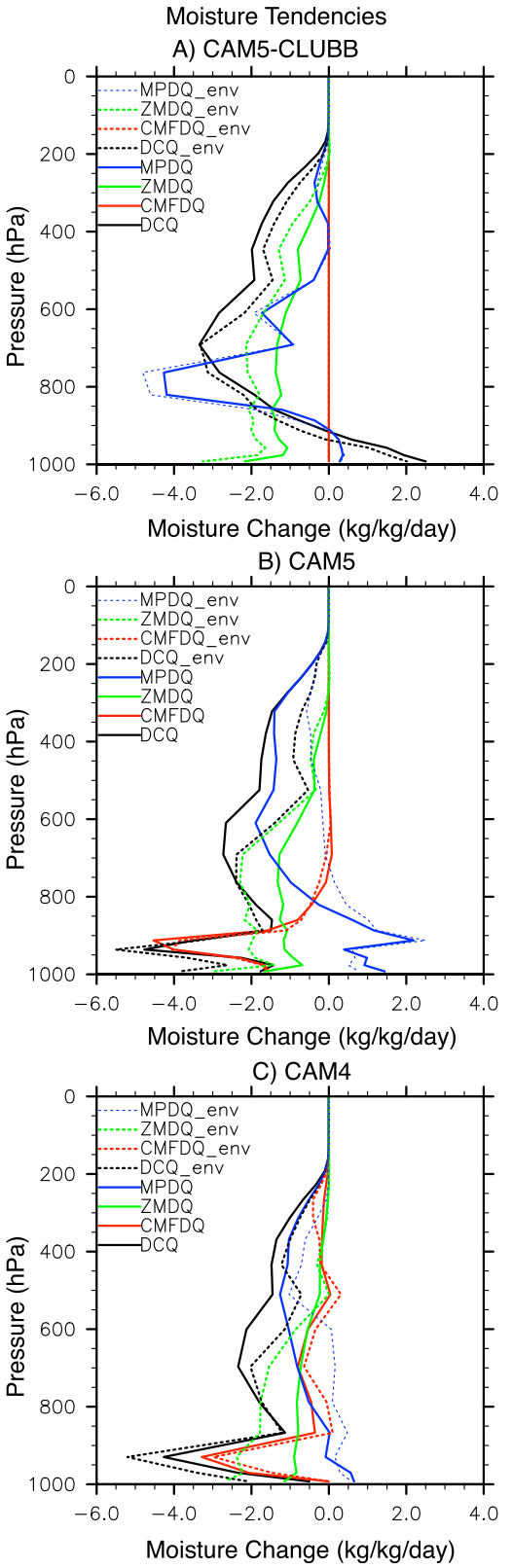

Figure 8. Humidity tendency profiles from (a) CAM-CLUBB, (b) CAM5, and (c) CAM4 averaged over 5°S–5°N inside (solid) and outside (dashed) the region of refinement. The tendency terms are DEEP convection (ZMDQ: green), shallow convection (CMFQ: red), large scale (macro and micro: MPDQ blue), and DCQ total (black).

form microphysics and CLUBB. The ZM humidity tendency does change, and it is balanced by a change in mixing (not shown in the moist physics tendencies).

The humidity tendencies are shown in Figure 8. CAM5-CLUBB (Figure 8a) has more similar humidity tendencies inside and outside the refined region (solid and dashed black lines) than does CAM5 or CAM4. CAM5 (Figure 8b) has very different performance (especially of the microphysics, blue), and note that the microphysics/macrophysics (MPDQ) and shallow convection (CMFDQ) are operating in opposition to each other: shallow convection seems to remove condensate that microphysics puts back. This may be a result of the coupling of the shallow convective detrainment in CAM5. Also note that CAM5-CLUBB has its main tendency for low clouds higher (800 hPa) than CAM4 or CAM5 (950 hPa).

In summary, the aquaplanet simulations indicate that CAM5-CLUBB and CAM5 have more consistent precipitation and process rates inside and outside the high-resolution region than does CAM4 physics.

3.3. Climate Simulations

We now move on to full climate simulations that include topography and an active land surface. We focus on the CAM5-CLUBB physics, and upgrade the physical parameterizations in addition to CLUBB to use versions that are part of CAM6 (new ice nucleation, new cloud microphysics, and modified aerosol model). This model formulation is a preliminary version of CAM6 (called CAM6α), using the land component CLM4 from CESM1. The resolution sensitivity of CAM6α is very similar to CAM5-CLUBB simulations. There are slightly different tuning parameters than the final version of CAM6, but the basic physics is the same, except for a new surface drag scheme which was not available. We focus now on a variable mesh over the Continental United States (CONUS) illustrated in Figure 1 and described in section 2.

Globally, the three simulations have very similar climates when evaluated using a multivariate skill score (see below). The stability of midlatitude climate metrics across resolutions shows low-resolution sensitivity (in a climate sense). A detailed analysis indicates however that the low resolution (ne30) and VR simulations perform slightly better against observations than the high-resolution (ne120) simulation. For example, the RMSE for annual precipitation rate against Global Precipitation Climatology Project (GPCP) rain rates is 0.93 mm d^{-1} for uniform ne30, 0.95 mm d^{-1} for VR but 1.12 mm d^{-1} for uniform ne120. This is also indicated by an overall multivariate skill score following Taylor (2001), including precipitation, cloud radiative effects, surface stress and temperature, and free tropospheric zonal wind. This is likely because CAM6α was developed and optimized at low resolution, and there are some differences with resolution (as noted above). This global optimization or tuning affects results below.

First, we assess the stability of seasonal means for important quantities in the variable mesh region. We analyze climatological biases relative to observations, to see if there are regional or coherent differences between simulations. We compare the simulations to a common metric. For climatological data, we use European Center Interim Reanalysis (ERAI) surface temperature (Ts) and precipitation data, averaged over the same 1980–2005 period. Data is gridded to $1^\circ \times 1^\circ$ for all simulations and ERAI before comparison. Figure 9 illustrates the percent difference between the CAM6α CONUS simulations and ERAI climatological precipitation means for summer (June–August). Over land, summer precipitation is well represented. There are biases over the Plains, with too much precipitation west of the Mississippi river. This bias is probably due to diurnal cycle firing too early and a dearth of propagating convective systems (see below). The Upper Midwest (Dakotas, Iowa, and Minnesota) is too dry (and warm, see below) in summer. This is likely due to a bias in clouds, which are also too low. The values indicate the percent root-mean-square difference (PRMSD) between each simulation and ERAI. The differences are 54% for ne120 (uniform high resolution), 46% for ne30 (uniform low resolution) and 30% for the variable mesh.

Why is CAM6α variable-resolution sometimes "better" than uniform high resolution? As noted above, the low resolution (ne30) and VR simulations are slightly better tuned globally than the high-resolution simulation, and this affects the overall climate metrics. Since the majority of the variable-resolution grid is at the same resolution as the low-resolution (ne30) simulation, the global mean climatologies should be closely matched in the absence of significant physical parameterization resolution sensitivities (Zarzycki et al., 2015). This also offers further support that the variable-resolution CESM framework is dynamically consistent across scales when compared to globally uniform resolution counterparts, particularly with the CAM6α configuration used here.

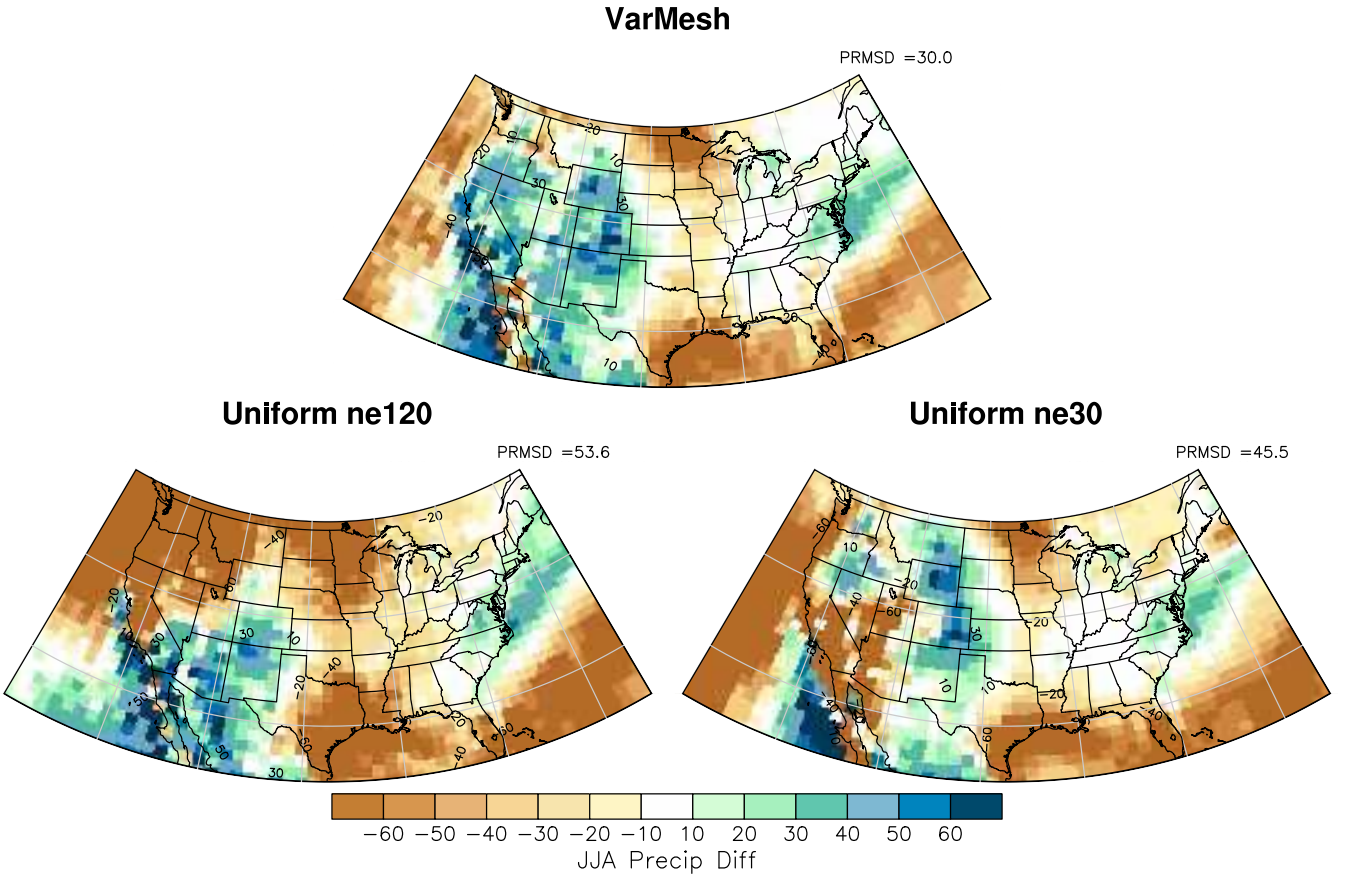

Figure 9. June–August percent difference between the CAM6α CONUS simulations and ERAI climatological precipitation means. The values indicate the percent root-mean-square difference (PRMSD) between each simulation and ERAI.

Figure 10 illustrates climatological precipitation anomalies for winter (December–February) relative to ERAI. The variable mesh in most respects looks like the ne120 simulation over land, with significant reductions in bias near the edges of the domain in the Pacific Northwest U.S., Texas, and the Upper Mid-west. Winter (DJF) differences from ERAI are significantly reduced in the Western U.S. due to better representation of mountain ranges. DJF values of the PRMSD are 17% (ne120), 20% (ne30), and 19% (VR).

Figure 11 illustrates summer (JJA) surface temperature (*Ts*) biases relative to ERAI. For all simulations, there is a 2–4°C positive bias in the Central U.S. in summer. This is a known bias in many models (Ma et al., 2014). The root-mean-square difference is 2.6°C for ne120, 2.1°C for ne30 but only 1.8°C for VR. The bias is due to a lack of cloud and less shortwave cloud radiative cooling in summer. *Ts* baises are higher in ne120, because of less cloud and less SW cloud radative effect. Biases are confined to the Upper Mid-west region, and are consistent with the dry bias to precipitation in this region (Figure 9) and may be coupled to the precipitation bias through land surface (soil moisture) feedbacks. The VR simulation does not reproduce the same midwest anomalies as uniform ne120 but has smaller anomalies, more similar to uniform ne30. This might be because of different large-scale forcing outside the region of refinement (lower climate biases in variable mesh and uniform ne30 than ne120). Winter (DJF) Ts biases (not shown) are generally $<$2°–3°. The model is slightly cooler over the northern Rockies with a warm anomaly in Nebraska, Kansas.

One of the major goals of high-resolution climate simulations is to represent the frequency of extreme events with high fidelity. To assess this, we look at statistics of high-frequency (3 hourly averages) summertime (JJA) temperature and precipitation. Frequency statistics are calculated on the native grid of each simulation. Since we are looking at frequency distributions, the exact grid for each data set is not important (the metric is frequency). For comparison to observations, it is difficult to find similar high-frequency

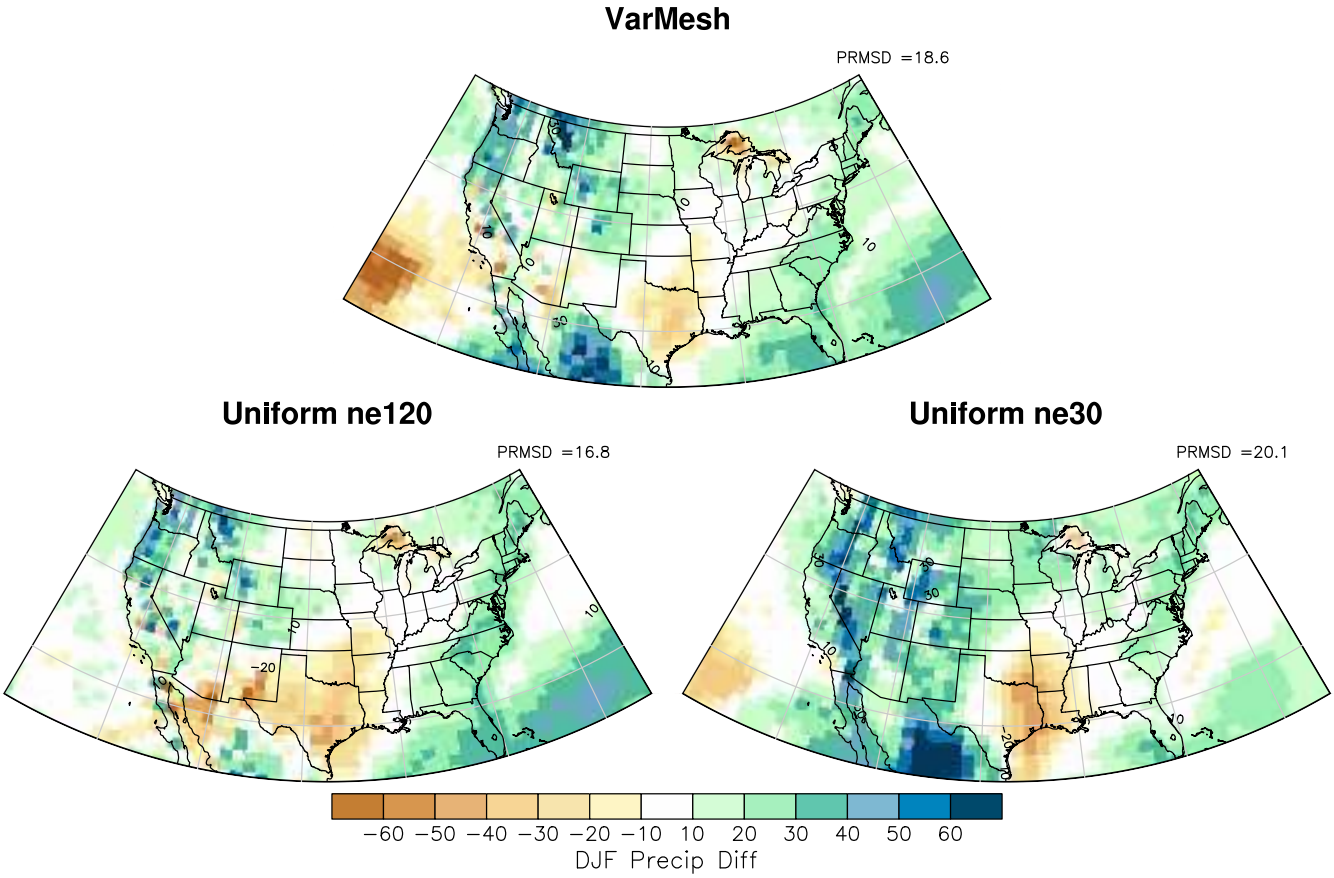

Figure 10. December–February percent difference between the CAM6α CONUS simulations and ERAI climatological precipitation means. The values indicate the percent root-mean-square difference (PRMSD) between each simulation and ERAI.

statistics. We use gridded CPC daily precipitation analyses (25 km, 0.25° resolution) for comparison (handled in methodology section) and also North American Regional Reanalyses (NARRs) for 3 hourly statistics. We note in particular that NARR analyses represent another model at ~32 km.

Figure 12 illustrates frequency distributions of precipitation. The VR simulation looks similar to the high-resolution intensities, and has higher extreme precipitation frequency than the low-resolution simulation, as expected. In winter (DJF, Figure 12 left), the frequency only extends to 200 mm d^{-1} and the variable mesh and high resolution are close to the CPC observations. Frequencies in summer go higher, and the variable mesh and high-resolution simulations have higher frequency of extreme precipitation (>300 mm d^{-1}). However, comparisons between gridded precipitation observations and high-resolution reanalysis may not be exact. Extreme precipitation frequency (>400 mm d^{-1}) may be too high in the high-resolution simulations relative to CPC precipitation analyses. The VR simulation is closer to observed intensities even in the high-resolution region, and the low resolution (Uniform 1d) is also closer to observations.

Perhaps the more focused question is whether the variable-resolution simulation reproduces the extremes seen in the high-resolution simulation at the finest scales. Figure 13 shows frequencies for 3 hourly average precipitation on the native grid of the simulations and the NARR reanalysis. Here high and variable-resolution simulations are producing the same statistics, all the way up to very infrequent and extreme precipitation values. The similarity indicates the variable mesh is successful at reproducing the statistics from the high-resolution simulation. Extreme precipitation frequencies are much higher than produced by NARR reanalyses. The extreme rain rates correspond to 150 mm in 3 h and are only sustained for 3 h. It does not imply that the model precipitates 1.2 m at a grid point in a day, rather 0.15 m in 3 h. Note that NARR is at slightly lower resolution but produces extremes closer to ne30, which may not be correct (too low).

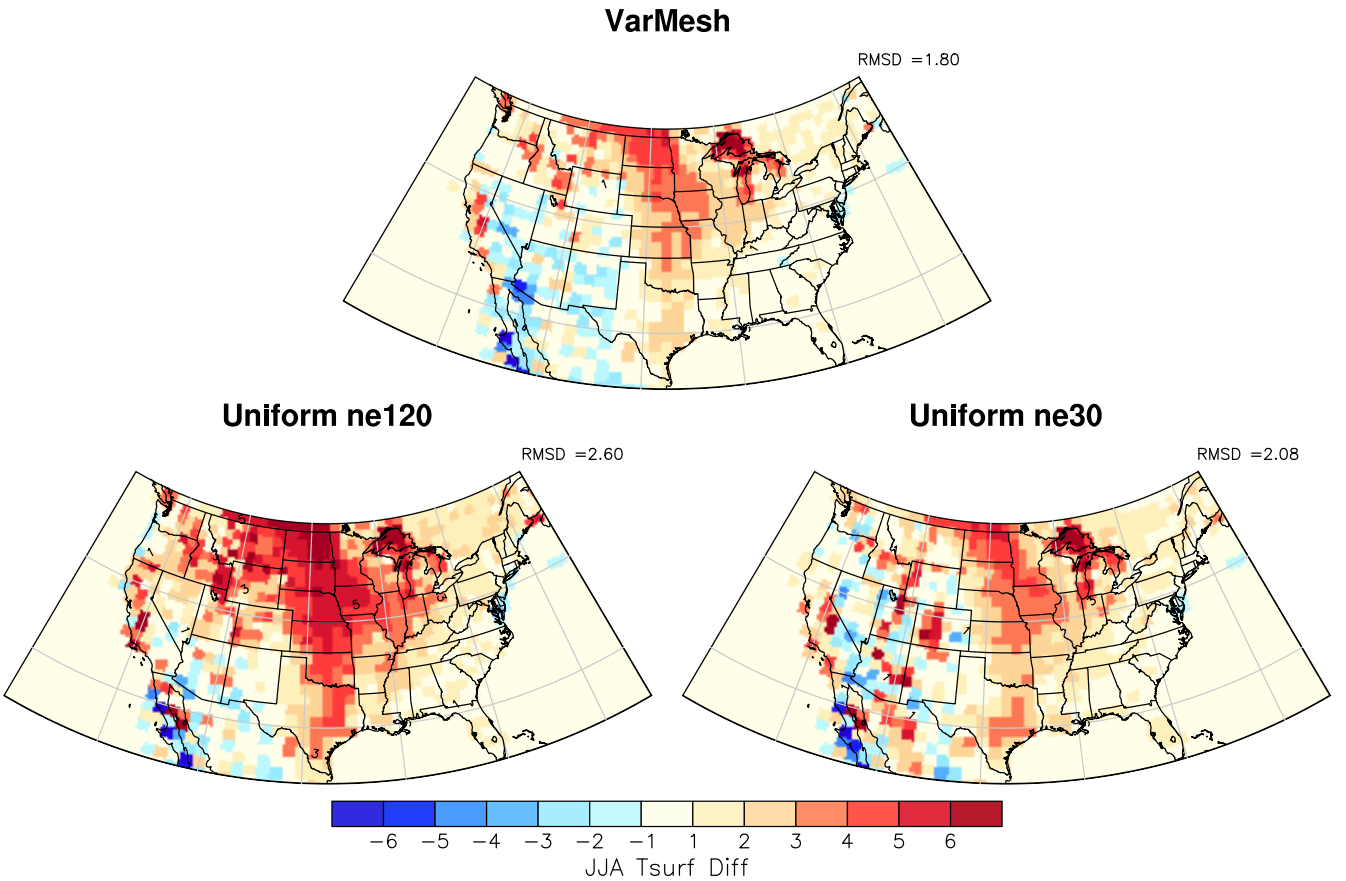

Figure 11. June–August difference between the CAM6α CONUS simulations and ERAI climatological mean surface temperature. The values indicate the root-mean-square difference (RMSD) between each simulation and ERAI.

Another metric for looking at the extremes is to integrate the frequency over the extremes and ask what is the frequency of exceedance of a threshold value for temperature or precipitation by integrating over the tail of the frequency distribution. This has the advantage of also having enough statistics to be able to look at interannual variability and changes in the exceedance frequency over time.

Figure 14 illustrates the frequency of exceedance of daily average summer (JJA) temperature above 307 K (34°C) from simulations. Because of the temperature bias in JJA of ∼2 K in the simulations, the frequency of

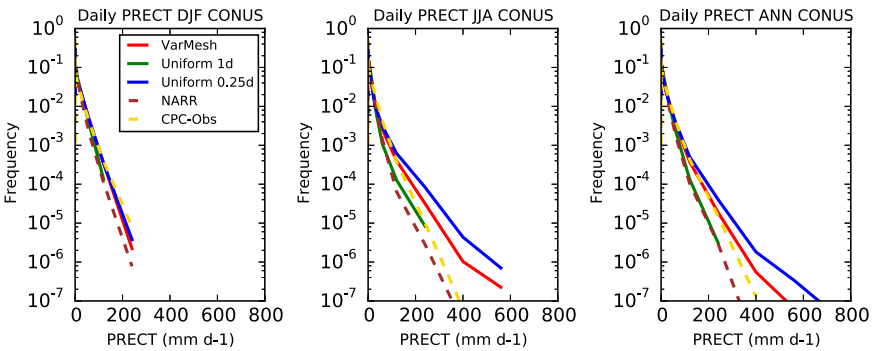

Figure 12. Daily Precipitation intensity histograms. Variable mesh (red solid), uniform high res (0.25°, blue solid), uniform low res (1° green solid) simulations and CPC observations (gold dash) and NARR reanalysis data (brown dash). The VR simulation looks similar to the high-resolution intensities and has higher extreme precipitation frequency than the low-resolution simulation.

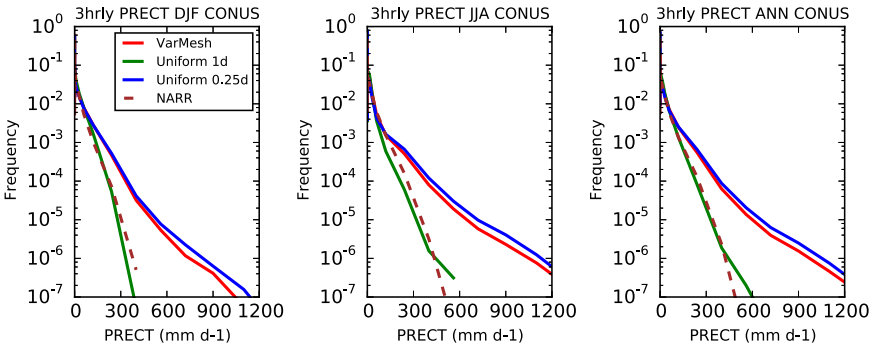

Figure 13. Precipitation intensity histograms from 3 hourly data (expressed in mm d^{-1}, but rates do not continue for a day). Variable mesh (red solid), Uniform high res (0.25°, blue solid), uniform low res (1° green solid) simulations and NARR reanalysis data (brown dash). VR simulations reproduce the uniform high-resolution frequencies.

exceedance above 305 K (32°C) is plotted for daily averaged ERAI 2m-temperature. All three simulations have similar exceedance probabilities, with the uniform high resolution about 0.02 (20%) higher. The variability from year to year is only about 20% of the value ($\sigma \sim 0.015$). ERAI has about the same interannual standard deviation ($\sigma = 0.012$), and the frequency of exceedence (when adjusted for the model temperature bias) is similar to the VR simulation. There is also an increasing trend in the frequency of extreme temperature in all the simulations (though not statistically significant). This is an indication of consistentcy with changes in recent climate records indicating more warm extremes (Meehl et al., 2009), but it is not a statistically significant trend as in observations. Note that this is the only metric from the simulations (or observations) that does show a trend, though not statistically significant.

Figure 15 shows exceedance probabilities for precipitation above 100 mm d^{-1} for 3 hourly (a, c) and daily (b, d) time frequencies. The VR simulation (blue) generally does a very good job of reproducing the high-resolution simulation (red) for both 3 hourly and daily frequencies (lower for daily). The low-resolution simulation (green) does not reproduce the frequency as well. In addition, the VR and high-resolution simulations also do a good job of reproducing the exceedance probability of daily precipitation relative to the CPC gridded precipitation observations. Since extreme precipitation impacts are a significant part of local and regional climate impacts, this is a significant achievement for trying to simulate regional climate extremes. There is large interannual variability, and no discernible trends.

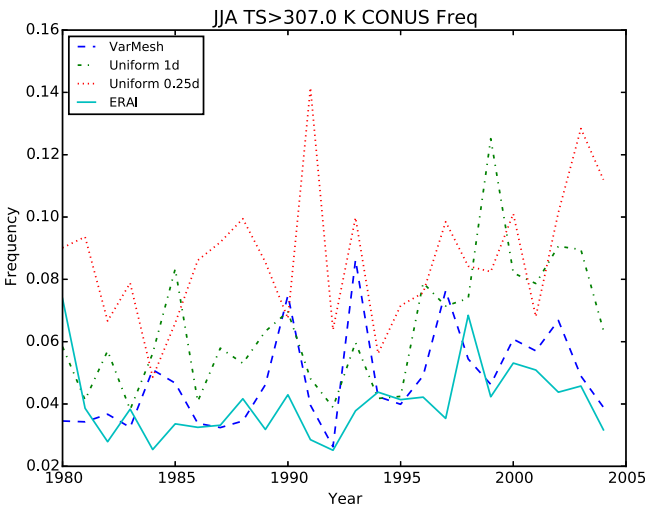

Figure 14. June–August (JJA) frequency of exceedance of daily average lowest level temperature above 307 K (34°C). Variable mesh (blue dash), uniform high res (0.25°, red dot), uniform low res (1° green dot dash) simulations. Also shown is frequency of daily ERAI interim reanalysis data 2 m temperature (solid cyan) above 305 K (32°C).

Figure 16 illustrates the diurnal cycle of precipitation rates in June from the Tropical Rainfall Measurement Mission (TRMM) satellite and model simulations. In Figure 16, the color indicates the local time of peak precipitation, and the intensity of the color the magnitude of the diurnal cycle. In June, satellite observations from TRMM illustrate that the peak in precipitation is around 1500LT at the edge of the Rocky Mountains, and then propagates later to the east, reaching the early morning near the Mississippi river. June is the peak for these systems. Afternoon storms dominate the mid-west of Illinois through Ohio, while a slightly earlier peak is seen from the Ozarks through the Appalacians, and the S. E. US see a peak near 1500–1800LT. The oceans feature a morning peak in the Gulf of Mexico and the Atlantic.

CAM simulations reproduce many of these features. This is new in CAM6α: earlier model versions had peaks in precipitation near noon LT, from a peak in convective precipitation (Gervais et al., 2014). The noon peak has been reduced in CAM6α, with evening peaks near the Rockies and in the Midwest. Propagating systems are not as evident, but there are hints of the systems in Nebraska in the variable mesh simulations (Figure 16b). The model reproduces the S.E. U.S. evening signal well. Notably, the intensities are weaker in the simulations than TRMM, but the VR simulation seems to have slightly more intense

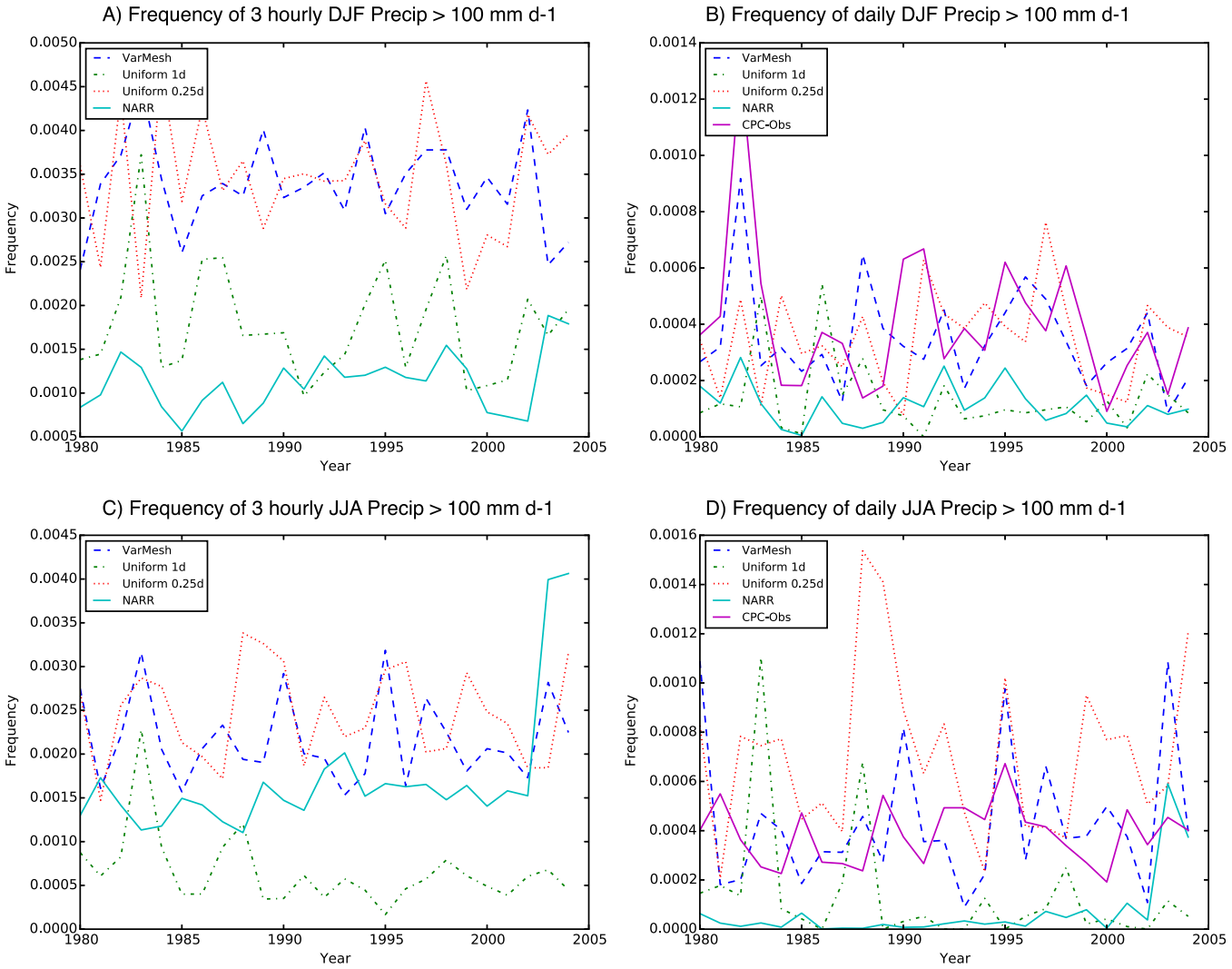

Figure 15. Frequency of exceedance of precipitation rates higher than 100 mm d^{-1} using (a, c) 3 hourly and (b, d) daily data for (a, b) December–February (DJF) and (c, d) June–August (JJA). Variable mesh (blue dash), uniform high res (0.25°, red dot), uniform low res (1° green dot dash) simulations, CPC observations (solid purple), and NARR reanalysis data (solid cyan).

cycles, and a better representation of the upper plains from Colorado to Montana. The overall fidelity is much better than in previous model versions.

4 .Summary/Conclusions

In this paper, we have presented a hierarchy of simulations using the regionally refined SE dynamical core in CAM. VR configurations reproduce the statistics of a high-resolution run well in baroclinic wave tests. This indicates that the variable-resolution mesh is producing "correct" dynamical flow solutions both inside and outside the refined region. However, there is damping of waves upstream in the low-resolution region that may affect the high-resolution region.

In midlatitude aquaplanet tests, the CAM physical parameterizations do have sensitivity to resolution. CAM4 has a big difference between high and low resolutions, and inside and outside a midlatitude refined mesh on an aquaplanet. CAM5 and CAM5-CLUBB have more similar performance inside and outside a refined mesh region, particularly for cloud radiative effects. This indicates that newer versions of the physical parameterizations (CAM5 and CAM5-CLUBB) are less sensitive to space and time scale resolution.

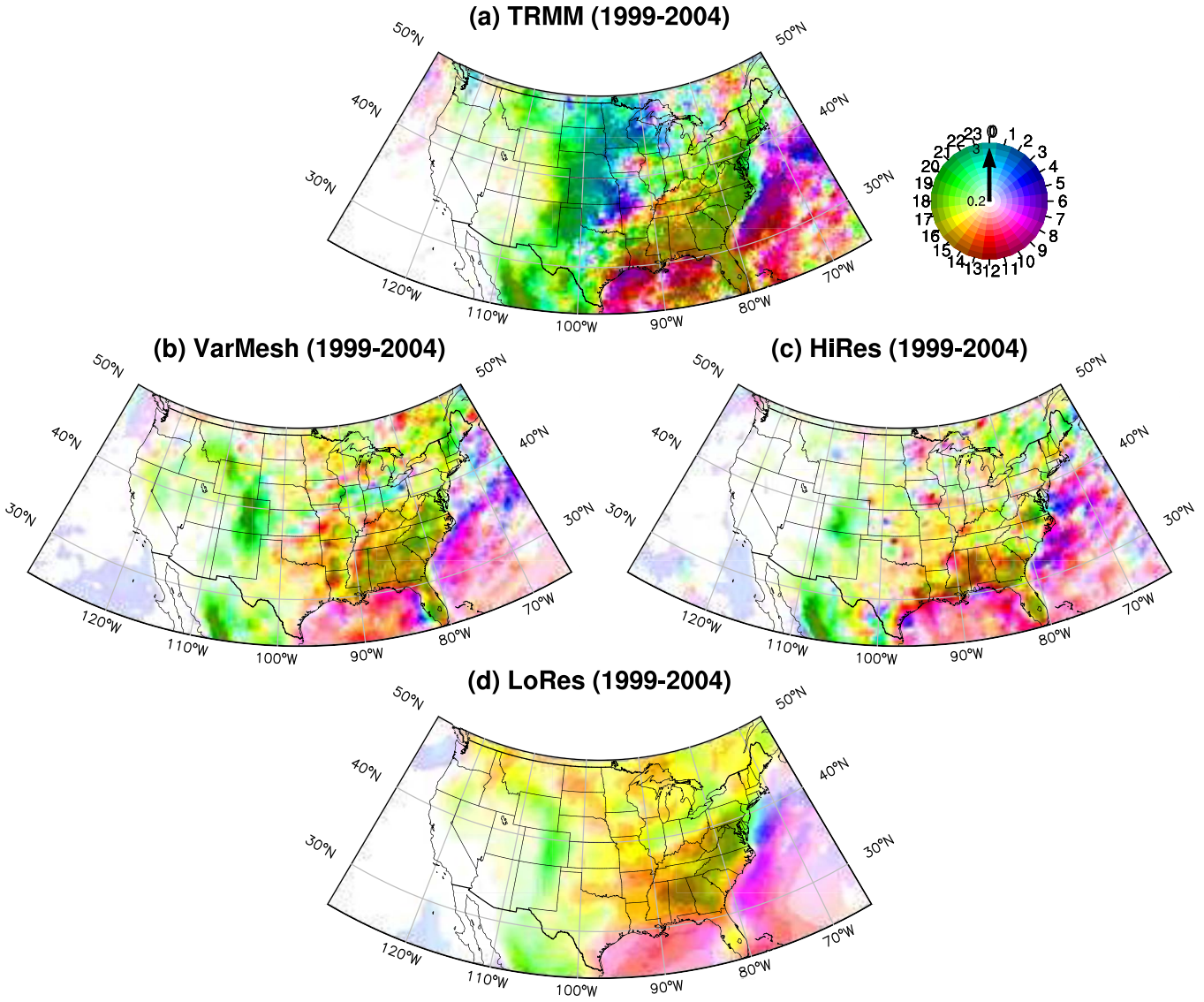

Figure 16. Diurnal cycle in June (6 year average from 1999 to 2004). (a) TRMM satellite observations, (b) variable mesh, (c) high resolution (ne120), and (d) low resolution (ne30). The local time peak of the diurnal cycle is shown in color on the color wheel. The intensity of the color is the amplitude.

In aquaplanet tests in the tropics, the CAM5-CLUBB configuration produces more similar precipitation amounts inside and outside the refined mesh region in the tropics, much better than CAM4 or CAM5 without CLUBB (Figure 5). There is still some compensation between large-scale and convective precipitation with CAM5-CLUBB, and this can be seen in the temperature and humidity tendency terms in aquaplanet simulations. But because CAM5-CLUBB has one less parameterization producing precipitation (no separate shallow convective scheme), there is less compensation between schemes.

The compensation is a feature of the CAM physical parameterization suite. Large-scale condensation is an instantaneous process that removes all liquid supersaturation whenever large-scale condensation, CLUBB and the prognostic cloud microphysics are run. In contrast, the convective parameterization has a time scale: it consumes instability and produces mass flux and precipitation at a defined rate. As the time step changes, the deep convective parameterization does less, and the large-scale condensation (including CLUBB and MG cloud microphysics) does more. This is a key feature of the model that has to be considered. Smaller grid boxes produce larger vertical velocities and hence more stratiform rain, that then reduces the moisture available for convection, which has a time scale. CAM6α uses similar schemes to CAM5-CLUBB, and global simulations indicate a similar, but low, scale sensitivity.

Variable mesh simulations can be an important tool for testing physical parameterizations across scales. The dynamics are stable, and the high-resolution regions resemble uniform high resolution in a baroclinic test case. In aquaplanet experiments for midlatitude storm tracks, broad scale measures of climate statistics (total cloud cover and longwave cloud radiative effect) are stable in both CAM5 and CAM5-CLUBB. Cloud forcing inside and outside refined regions in CAM5-CLUBB is stable to within 0.2 W m^{-2}. In tropical experiments, all configurations with a common deep convection scheme have decreased convective precipitation in the refined (high-resolution) region. The stratiform precipitation is increased in the high-resolution region. However, in CAM5-CLUBB, the balance of the two produces more similar total precipitation inside and outside a refined mesh region in the convergence on the equator: better than either CAM4 or CAM5. The total heating and moistening tendencies in the near equatorial region are nearly the same inside and outside the refined mesh region in CAM5-CLUBB, more so than CAM5 or CAM4.

Finally, we have conducted detailed simulations with full physics and a refined mesh over the Continental United States (CONUS) with CAM6α. We use a smaller time step appropriate to the finest resolution for the simulations, and do limited tuning. Results indicate that for most metrics, the VR simulation reproduces high-resolution high-frequency statistics for temperature, precipitation and clouds in the CONUS region. This is clear for example in winter orographic precipitation in the western US. In addition, the model performs well against observations, including observations of extreme precipitation frequency. Some local precipitation values are high, and there remains a positive bias in summertime surface temperature, that is coupled to biases in clouds and precipitation. Some of the bias patterns in VR simulations resemble the lower-resolution mesh, which may indicate that they result also from large-scale forcing outside the refined region.

By some metrics, the VR simulations have smaller biases than uniform high-resolution simulations. This is possible because the mean VR global climate tends to be dominated by the low-resolution region. The CAM6α physics is optimized (tuned) for this low resolution, thus there still is some minor scale sensitivity (although much less than CAM4).

Overall, at all stages from baroclinic wave tests to aquaplanet to full physics, we have tested CAM variable-resolution simulations against uniform high-resolution meshes (the "reference" case). We find that CAM5 and CAM5-CLUBB provides better stability across resolutions than CAM4. The variable mesh CAM6α version used here can accurately reproduce the climate statistics of the high-resolution mesh in the high-resolution region. The variable-resolution mesh also reproduces observed features of extreme precipitation, and all simulations produce a trend in extreme temperatures in summer, but no trends in extreme precipitation over the period 1980–2005.

Global climate metrics carry through into the high-resolution region. Global biases in low resolution (ne30) and variable mesh are lower than the high-resolution (ne120) simulation, and this can result in lower biases in the high-resolution region. Indicating that the high-resolution region does feel the global climate metrics, and adjustments to match observations. VR simulations may have distinct advantages for climate simulation over uniform high resolution if the model is better optimized (tuned) for lower resolution.

Thus, the variable-resolution framework with physics that is stable across resolutions can accurately reproduce regional climate statistics of a high-resolution simulation. CAM6α with the spectral element dynamical core is such a model. This does not require nesting (which requires more computational points), or forcing multiple models, and is thus an energetically consistent approach for efficient high-resolution regional climate simulation. It works similar to a two way nest (where the small scale feeds back on the large scale), with lower computational expense, and reduced complexity of "merging" a nested domain into a lower-resolution domain.

Acknowledgments
The National Center for Atmospheric Research is Sponsored by the U.S. National Science Foundation. Computer Resources provided by CHAP and ASD awards. This work was supported at NCAR by a U.S. National Science Foundation (NSF) grant for a Climate Process Team (CPT) on cloud-aerosol interactions (AGS-0968640), A NSF Earth System Modeling (EaSM) grant on multiscale modeling (AGS-1049057) and a U.S. Department of Energy SciDAC grant on Tropical Biases (DE-SC0006702). Model output from the simulations (climatologies and summary statistics) are available upon inquiry to the corresponding author. Model code will be released in CESM2.

References

Bacmeister, J. T., Reed, K. A., Hannay, C., Lawrence, P., Bates, S., Truesdale, J. E., et al. (2016). Projected changes in tropical cyclone activity under future warming scenarios using a high-resolution climate model. *Climatic Change*, *146*, 1–14. https://doi.org/10.1007/s10584-016-1750-x

Bacmeister, J. T., Wehner, M. F., Neale, R. B., Gettelman, A., Hannay, C., Lauritzen, P. H., et al. (2014). Exploratory high-resolution climate simulations using the Community Atmosphere Model (CAM). *Journal of Climate*, *27*(9), 3073–3099. https://doi.org/10.1175/JCLI-D-13-00387.1

Bogenschutz, P. A., Gettelman, A., Morrison, H., Larson, V. E., Craig, C., & Schanen, D. P. (2013). Higher-order turbulence closure and its impact on climate simulation in the Community Atmosphere Model. *Journal of Climate*, *26*(23), 9655–9676. https://doi.org/10.1175/JCLI-D-13-00075.1

Bogenschutz, P. A., Krueger, S. K., & Khairoutdinov, M. (2010). Assumed probability density functions for shallow and deep convection. *Journal of Advances in Modeling Earth Systems*, *2*, 10. https://doi.org/10.3894/JAMES.2010.2.10

Chen, M., Shi, W., Xie, P., Silva, V. B. S., Kousky, V. E., Wayne Higgins, R., et al. (2008). Assessing objective techniques for gauge-based analyses of global daily precipitation. *Journal of Geophysical Research*, *113*, D04110. https://doi.org/10.1029/2007JD009132

Dee, D. P., Uppala, S. M., Simmons, A. J., Berrisford, P., Poli, P., Kobayashi, S., et al. (2011). The ERA-Interim reanalysis: Configuration and performance of the data assimilation system. *Quarterly Journal of the Royal Meteorological Society*, *137*(656), 553–597. https://doi.org/10.1002/qj.828

Gent, P. R., Danabasoglu, G., Donner, L. J., Holland, M. M., Hunke, E. C., Jayne, S. R., et al. (2011). The Community Climate System Model Version 4. *Journal of Climate*, *24*(19), 4973–4991. https://doi.org/10.1175/2011JCLI4083.1

Gervais, M., Gyakum, J. R., Atallah, E., Tremblay, L. B., & Neale, R. B. (2014). How well are the distribution and extreme values of daily precipitation over North America represented in the Community Climate System Model? A comparison to reanalysis, satellite, and gridded station data. *Journal of Climate*, *27*(14), 5219–5239. https://doi.org/10.1175/JCLI-D-13-00320.1

Gettelman, A. (2015). Putting the clouds back in aerosol–cloud interactions. *Atmospheric Chemistry and Physics*, *15*(21), 12397–12411. https://doi.org/10.5194/acp-15-12397-2015

Gettelman, A., & Morrison, H. (2015). Advanced two-moment bulk microphysics for global models. Part I: Off-line tests and comparison with other schemes. *Journal of Climate*, *28*(3), 1268–1287. https://doi.org/10.1175/JCLI-D-14-00102.1

Golaz, J.-C., Larson, V. E., & Cotton, W. R. (2002). A PDF-based model for boundary layer clouds. Part II: Model results. *Journal of the Atmospheric Sciences*, *59*, 3552–3571.

Guba, O., Taylor, M. A., Ullrich, P. A., Overfelt, J. R., & Levy, M. N. (2014). The spectral element method (SEM) on variable-resolution grids: Evaluating grid sensitivity and resolution-aware numerical viscosity. *Geoscientific Model Development*, *7*(6), 2803–2816. https://doi.org/10.5194/gmd-7-2803-2014

Hack, J. J. (1994). Parameterization of moist convection in the National Center for Atmospheric Research community climate model (CCM2). *Journal of Geophysical Research*, *99*(D3), 5551–5568. https://doi.org/10.1029/93JD03478

Harris, L. M., & Lin, S.-J. (2013). A two-way nested global-regional dynamical core on the cubed-sphere grid. *Monthly Weather Review*, *141*(1), 283–306.

Huang, X., Rhoades, A. M., Ullrich, P. A., & Zarzycki, C. M. (2016). An evaluation of the variable-resolution CESM for modeling California's climate. *Journal of Advances in Modeling Earth Systems*, *8*, 345–369. https://doi.org/10.1002/2015MS000559

Hurrell, J. W., Holland, M., Gent, P., Ghan, S., Kay, J. E., Kushner, P., et al. (2013). The Community Earth System Model: A framework for collaborative research. *Bulletin of the American Meteorological Society*, *94*(9), 1339–1360. https://doi.org/10.1175/BAMS-D-12-00121.1

Jablonowski, C., & Williamson, D. L. (2006). A baroclinic instability test case for atmospheric model dynamical cores. *Quarterly Journal of the Royal Meteorological Society*, *132*, 2943–2975. https://doi.org/10.1256/qj.06.12

Kummerow, C., Barnes, W., Kozu, T., Shiue, J., & Simpson, J. (1998). The Tropical Rainfall Measuring Mission (TRMM) sensor package. *Journal of Atmospheric and Oceanic Technology*, *15*(3), 809–817. https://doi.org/10.1175/1520-0426(1998)015<0809:TTRMMT>2.0.CO;2

Laprise, R. (2008). Regional climate modelling. *Journal of Computational Physics*, *227*(7), 3641–3666. https://doi.org/10.1016/j.jcp.2006.10.024

Larson, V. E., Golaz, J.-C., & Cotton, W. R. (2002). Small-scale and mesoscale variability in cloudy boundary layers: Joint probability density functions. *Journal of the Atmospheric Sciences*, *59*(24), 3519–3539. https://doi.org/10.1175/1520-0469(2002)059<3519:SSAMVI>2.0.CO;2

Lauritzen, P. H., Bacmeister, J. T., Callaghan, P. F., & Taylor, M. A. (2015). NCAR_Topo (v1.0): NCAR global model topography generation software for unstructured grids. *Geoscientific Model Development*, *8*(12), 3975–3986. https://doi.org/10.5194/gmd-8-3975-2015

Lauritzen, P. H., Nair, R. D., Herrington, A. R., Callaghan, P., Goldhaber, S., Dennis, J. M., et al. (2018). NCAR CESM2.0 release of CAM-SE: A reformulation of the spectral-element dynamical core in dry-mass vertical coordinates with comprehensive treatment of condensates and energy, *Journal of Advances in Modeling Earth Systems*, *10*. https://doi.org/10.1002/2017MS001275

Ma, H.-Y., Xie, S., Klein, S. A., Williams, K. D., Boyle, J. S., Bony, S., et al. (2014). On the correspondence between mean forecast errors and climate errors in CMIP5 models. *Journal of Climate*, *27*(4), 1781–1798. https://doi.org/10.1175/JCLI-D-13-00474.1

McGregor, J. L. (1997). Regional climate modelling. *Meteorology and Atmospheric Physics*, *63*(1–2), 105–117. https://doi.org/10.1007/BF01025367

Mearns, L. O., Arritt, R., Biner, S., Bukovsky, M. S., McGinnis, S., Sain, S., et al. (2012). The North American regional climate change assessment program: Overview of phase I results. *Bulletin of the American Meteorological Society*, *93*(9), 1337–1362. https://doi.org/10.1175/BAMS-D-11-00223.1

Meehl, G. A., Tebaldi, C., Walton, G., Easterling, D., & McDaniel, L. (2009). Relative increase of record high maximum temperatures compared to record low minimum temperatures in the U.S. *Geophysical Research Letters*, *36*, L23701. https://doi.org/10.1029/2009GL040736

Mesinger, F., DiMego, G., Kalnay, E., Mitchell, K., Shafran, P. C., Ebisuzaki, W., et al. (2006). North American Regional Reanalysis. *Bulletin of the American Meteorological Society*, *87*(3), 343–360. https://doi.org/10.1175/BAMS-87-3-343

Neale, R. B., Chen, C. C., Gettelman, A., Lauritzen, P. H., Park, S., Williamson, D. L., et al. (2010). *Description of the NCAR Community Atmosphere Model (CAM5.0)* (Tech. Rep. NCAR/TN-486+STR). Boulder, CO: National Center for Atmospheric Research.

Neale, R. B., Richter, J., Park, S., Lauritzen, P. H., Vavrus, S. J., Rasch, P. J., et al. (2013). The mean Climate of the Community Atmosphere Model (CAM4) in forced SST and fully coupled experiments. *Journal of Climate*, *26*(14), 5150–5168. https://doi.org/10.1175/JCLI-D-12-00236.1

Neale, R. B., Richter, J. H., & Jochum, M. (2008). The impact of convection on ENSO: From a delayed oscillator to a series of events. *Journal of Climate*, *21*, 5904. https://doi.org/10.1175/2008JCLI2244.1

Park, S., & Bretherton, C. S. (2009). The University of Washington shallow convection and moist turbulence schemes and their impact on climate simulations with the Community Atmosphere Model. *Journal of Climate*, *22*, 3449–3469.

Rauscher, S. A., Ringler, T. D., Skamarock, W. C., & Mirin, A. A. (2012). Exploring a global multiresolution modeling approach using aquaplanet simulations. *Journal of Climate*, *26*(8), 2432–2452. https://doi.org/10.1175/JCLI-D-12-00154.1

Rhoades, A. M., Huang, X., Ullrich, P. A., & Zarzycki, C. M. (2016). Characterizing Sierra Nevada snowpack using variable-resolution CESM. *Journal of Applied Meteorology and Climatology*, *55*(1), 173–196. https://doi.org/10.1175/JAMC-D-15-0156.1

Ringler, T. D., Jacobsen, D., Gunzburger, M., Ju, L., Duda, M., & Skamarock, W. (2011). Exploring a multiresolution modeling approach within the shallow-water equations. *Monthly Weather Review*, *139*(11), 3348–3368. https://doi.org/10.1175/MWR-D-10-05049.1

Sakaguchi, K., Leung, L. R., Zhao, C., Yang, Q., Lu, J., Hagos, S., et al. (2015). Exploring a multi-resolution approach using AMIP simulations. *Journal of Climate*, *28*, 5549–5574. https://doi.org/10.1175/JCLI-D-14-00729.1

Small, R. J., Bacmeister, J., Bailey, D., Baker, A., Bishop, S., Bryan, F., et al. (2014). A new synoptic scale resolving global climate simulation using the Community Earth System Model. *Journal of Advances in Modeling Earth Systems*, *6*, 1065–1094. https://doi.org/10.1002/2014MS000363

Taylor, K. E. (2001). Summarizing multiple aspects of model performance in a single diagram. *Journal of Geophysical Research*, *106*(D7), 7183–7192. https://doi.org/10.1029/2000JD900719

Taylor, M. A. (2011). Conservation of mass and energy for the moist atmospheric primitive equations on unstructured grids. In P. Lauritzen, C. Jablonowski, M. Taylor, & R. Nair (Eds.), *Numerical techniques for global atmospheric models* (pp. 357–380). Berlin, Germany: Springer. https://doi.org/10.1007/978-3-642-11640-7-12

Wehner, M. F., Reed, K. A., Li, F., Prabhat, Bacmeister, J., Chen, C.-T., et al. (2014). The effect of horizontal resolution on simulation quality in the Community Atmospheric Model, CAM5.1. *Journal of Advances in Modeling Earth Systems*, *6*, 980–997. https://doi.org/10.1002/2013MS000276

Williamson, D. L. (2008). Convergence of aqua-planet simulations with increasing resolution in the Community Atmospheric Model, Version 3. *Tellus, Series A*, *60*, 848–862.

Wu, C., Liu, X., Lin, Z., Rhoades, A. M., Ullrich, P. A., Zarzycki, C. M., et al. (2017). Exploring a variable-resolution approach for simulating regional climate in the Rocky Mountain region using the VR-CESM. *Journal of Geophysical Research: Atmospheres*, *122*, 10939–10965. https://doi.org/10.1002/2017JD027008

Zarzycki, C. M., & Jablonowski, C. (2014). A multidecadal simulation of Atlantic tropical cyclones using a variable-resolution global atmospheric general circulation model. *Journal of Advances in Modeling Earth Systems*, *6*, 805–828. https://doi.org/10.1002/2014MS000352

Zarzycki, C. M., & Jablonowski, C. (2015). Experimental tropical cyclone forecasts using a variable-resolution global model. *Monthly Weather Review*, *143*(10), 4012–4037. https://doi.org/10.1175/MWR-D-15-0159.1

Zarzycki, C. M., Jablonowski, C., & Taylor, M. A. (2014b). Using variable-resolution meshes to model tropical cyclones in the Community Atmosphere Model. *Monthly Weather Review*, *142*(3), 1221–1239. https://doi.org/10.1175/MWR-D-13-00179.1

Zarzycki, C. M., Jablonowski, C., Thatcher, D. R., & Taylor, M. A. (2015). Effects of localized grid refinement on the general circulation and climatology in the Community Atmosphere Model. *Journal of Climate*, *28*(7), 2777–2803. https://doi.org/10.1175/JCLI-D-14-00599.1

Zarzycki, C. M., Levy, M. N., Jablonowski, C., Overfelt, J. R., Taylor, M. A., & Ullrich, P. A. (2014a). Aquaplanet experiments using CAM's variable-resolution dynamical core. *Journal of Climate*, *27*(14), 5481–5503. https://doi.org/10.1175/JCLI-D-14-00004.1

Zhang, G. J., & McFarlane, N. A. (1995). Sensitivity of climate simulations to the parameterization of cumulus convection in the Canadian Climate Center general circulation model. *Atmosphere-Ocean*, *33*, 407–446.